We are IntechOpen, the world's leading publisher of Open Access books
Built by scientists, for scientists

4,800
Open access books available

122,000
International authors and editors

135M
Downloads

154
Countries delivered to

Our authors are among the

TOP 1%
most cited scientists

12.2%
Contributors from top 500 universities

BOOK CITATION INDEX
CLARIVATE ANALYTICS
INDEXED

WEB OF SCIENCE™

Selection of our books indexed in the Book Citation Index
in Web of Science™ Core Collection (BKCI)

Interested in publishing with us?
Contact book.department@intechopen.com

Numbers displayed above are based on latest data collected.
For more information visit www.intechopen.com

Preparation and Numerical Modelling of Ceramic Foam Insulation for Energy Saving in Buildings

Ru Ji, Xidong Wang and Yang He

Abstract

For the purpose of energy saving in buildings, a foam ceramic insulation (FCI) was prepared by using fly ash (FA) and ceramic waste (CW) as the main raw materials for its matrix part and foam part, respectively. The effects of the sintering temperature and the additive agent on the macroscopic performances were systematically measured and investigated. The experiment results indicate that for the matrix sample 5% quartz addition makes the rupture modulus at 1200°C reach high to 34.28 MPa, while the corresponding water absorption capacity is only 0.83%. In addition, for the foam sample with 1 wt% silicon carbide, the lowest measured bulk density and thermal conductivity at 1200°C are 0.471 g/cm^3 and 0.1184 W/(m•K), respectively. Furthermore, the proposed simulation model predicts that the effective thermal conductivity of FCI decreases with the decrease of the bulk density. Moreover, the simulation results calculated by EnergyPlus software indicate that the synthetic FCI can efficiently reduce the building's heating and cooling loads and exerts excellent energy conservation effect.

Keywords: ceramic foam insulation, solid waste, numerical modelling, thermal conductivity, energy saving in buildings

1. Introduction

It is well known that as the society and economy is developing at a high rate, about 35% of the total energy is consumed by buildings [1–4]. For the sake of energy saving in buildings, all over the world, there are many different concepts of energy-efficient buildings, such as passive houses, near-zero-energy buildings, and even active houses [5]. According to the requirements of these houses' design, the energy use in these buildings needs to be strictly reduced to a very certain small range. Therefore, an appropriate thermal insulation material is necessary to

realise the energy saving in buildings [6]. As ceramic foam insulation (CFI) is one of the notable methods to reduce the energy use in buildings, it has been widely developed in recent years.

As we all know, the building insulation materials are generally sorted into two groups, organic insulation materials and inorganic insulation materials. Organic insulation materials, such as polystyrene foam, often lead to a series of problems related to combustion, environmental toxicity, and adhesive incompatibility with cement and ceramic structures. In addition, organic insulation materials usually exert short working life, for instance, foam plastic only can ensure the required heat resistance in about 8 years. However, inorganic materials, such as CFI, are excellent building insulation materials, which have many advantages compared with other thermal insulation materials, including chemically inactive, noncombustible, low moisture absorption, chemically stable, long-time stable in physical properties, environmental friendly, and long use life [7]. For the above reasons, this study is motivated to propose a novel FCI for saving energy in buildings.

On the other hand, according to the investigation in literature, it is known to us that the traditional manufacture of ceramic materials often requires massive amount of natural raw materials, such as clay and feldspar [8–10]. However, recently, taking into consideration the big challenges in environmental protection and energy saving, nontraditional raw materials are needed in the synthesis process of the ceramic materials. Therefore, the development of innovative ceramic materials by using huge amounts of alternative raw materials, especially solid waste, will be important to the environmental protection.

Hence, in this research, according to our previous work [11–13], two solid wastes were applied as the main raw materials for the synthesis of FCI. Firstly, fly ash (FA), a by-product of thermal generation in coal power stations, is used as the main raw material in the matrix part of the FCI [14]. According to the statistics, more than 750 million tonnes of FA are generated each year, but only less than 50% of FA is utilised. In China, the annual output of FA reached almost 600 million tonnes, which results in very serious environmental pollution, such as groundwater contamination [15–17]. Secondly, the reclaimed waste is the ceramic waste (CW). Statistics show that in the ceramic industry about 30% of the daily production will turn into solid waste. As we all know, CW is not recycled in any form at present [18]. Therefore, both solid wastes will cause serious environmental pollution [19–20]. So it is necessary to develop an effective way to recycle FA and CW.

Based on the previous work of our research [11–13], we are therefore motivated to prepare FCI by using FA and CW as the main raw materials. Moreover, since the study of heat transfer behaviour of FCI and its energy-saving function in buildings was important to guide the synthesis process of FCI, in this study, the foaming behaviour, the thermal conductivity, and its energy-saving function were investigated experimentally and were modelled by simulative method.

2. Experimental methods

2.1. Materials

For the manufacture of CFI boards the raw materials can be divided into two kinds, matrix raw materials and foam raw materials. Firstly, the matrix raw materials were composed of

FA, clay, feldspar, and quartz, which were all driven from the same region in China. Secondly, the foam raw materials included CW and other additives. Here, CW was used as a main raw material and SiC was applied as a foaming agent. The chemical characteristics of the main raw materials were measured by X-ray fluorescence (XRF) scan and are shown in **Table 1**. It can be seen that for all main raw materials, SiO_2 and Al_2O_3 possess the dominating proportions with the total proportion of 81.87, 71.53, 86.10, 95.77 and 84.01 wt%. It is interesting to note that for feldspar the total contents of K_2O and Na_2O are high: 11.72 wt%.

In addition, the crystalline phases of the raw materials are determined by X-ray diffraction (XRD) (D/MAX-PC 2500, Rigaku), and the XRD patterns are presented in **Figure 1**. It can be seen that FA is a heterogeneous material. Firstly, the major crystalline phases of FA are quartz and mullite with a small amount of gypsum. Secondly, it is interesting to note that parts of FA belong to the amorphous phase due to the observed low and broad diffraction bands in the range of 20–30°. Moreover, for CW, the main structure is quartz.

2.2. Preparation

In this research, for the matrix part, 50 wt% FA will be used as the main raw material in all batches. While, for the foam part, only CW will be utilised as the raw material with only 1% SiC. In this study, according to the previous work, the detailed steps of the preparation are shown as follows.

Firstly, all raw materials were thoroughly mixed and milled in the proportion as shown in **Table 2**. Here, quartz content in the batches 1–5 varied from 0 to 20 wt%. Then, mixtures were wet ground in two ball mills for 15 h to obtain the homogeneous slurries. The slurries were sieved to pass through a 200-mesh screen and dried at 110°C for 12 h. Subsequently, the two mixtures were granulated in a moist condition and samples were hydraulically compacted using uniaxial pressing at 10 MPa. Finally, the shaped samples were dried at 105°C for 3 h, followed by calcination in a muffle furnace at the preset sintering temperature, and the sintered samples were cooled naturally.

2.3. Characterisation

For the matrix part, the obtained samples were measured for moisture absorption (MA) capacity and rupture modulus.

Content (wt%)	SiO_2	Al_2O_3	K_2O	Na_2O	CaO	Fe_2O_3	MgO	TiO_2	S	LOI
Fly ash	41.97	39.90	0.50	0.20	6.41	1.96	0.60	1.20	3.15	3.64
Clay	34.96	36.57	0.39	0.09	0.49	0.82	0.22	1.47	—	24.38
Feldspar	68.60	17.50	7.74	3.98	0.53	0.41	0.17	0.04	—	0.83
Quartz	91.30	4.47	1.76	1.19	0.42	0.17	0.15	0.01	—	0.44
Ceramic waste	65.18	18.83	1.61	4.10	1.61	0.45	3.22	0.21	—	4.13

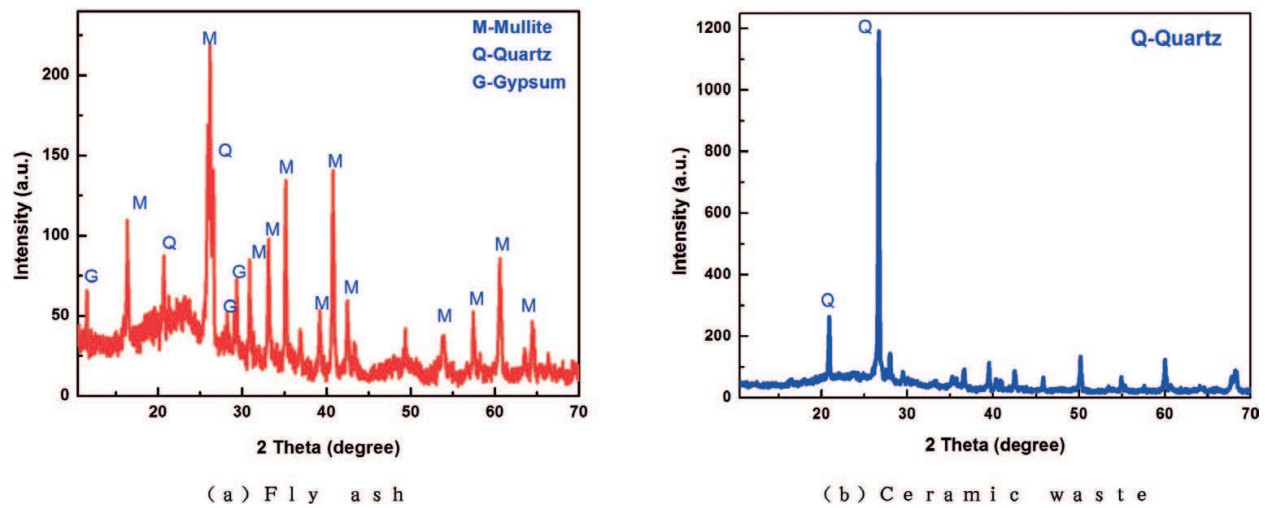**Table 1.** Chemical composition of main raw materials.

Figure 1. XRD patterns of the main raw materials.

The moisture absorption (MA) capacity was tested according to the following method. Firstly, the dried mass of the sintered sample (M_d, kg) was measured. Secondly, the sample was put into boiled water for 5 h and then was soaked for another 24 h. Finally, in water, the mass of the suspended sample (M_{s1}, kg) was determined, and the saturated mass (M_{s2}, kg) was measured. So MA (%) can be obtained as follows:

$$MA = \frac{M_{s2} - M_d}{M_d} \times 100 \tag{1}$$

The rupture modulus, R (MPa), is calculated by the following formula:

$$R = \frac{3Fl}{2\,bh^2} \tag{2}$$

where F is the failing load (N); l is the distance between two support bars (mm); b is the width of the specimen (mm); and h is the minimum thickness of the sample (mm).

For the foam part, the sintered samples were tested regarding bulk density and measured thermal conductivity.

		No. 1	No. 2	No. 3	No. 4	No. 5	No. 6
Matrix part	Fly ash	50	50	50	50	50	—
	Clay	20	20	20	20	20	—
	Feldspar	30	25	20	15	10	—
	Quartz	—	5	10	15	20	—
Foam part	Ceramic waste	—	—	—	—	—	100
	SiC	—	—	—	—	—	1

Table 2. Batch compositions of the samples (wt%).

The bulk density (ρ_b) of final sintered sample was determined by referencing the Chinese Standards Specifications. In particular, three parameters were detected. Firstly, the sintered samples were dried at 110°C for 24 h and then restored to room temperature in a balance desiccator. In this status, the specimen's weight was accurately measured, M_a. Secondly, the samples were immersed in boiled water for 3 h, then removed the heating and made samples to still stay in the water for 1 h. Samples' weight M_b in the water was measured by hanging on the hook of the precision electronic balance. Thirdly, after the above process, samples were taken out of the water and the redundant water on the surface was wiped using a wet cloth. Then, the weight M_c of the sample was measured. Finally, the bulk density was calculated by using the following formula, in which ρ_{water} was the density of water.

$$\rho_b = \frac{M_a}{M_b - M_c} \times \rho_{water} \tag{3}$$

For thermal conductivity measurements, a series of rectangular briquettes were prepared separately. The thermal conductivities of the samples were measured in a vapour-tight envelope by using a guarded hotplate apparatus (IMDRY3001-II). For the experiment, the hotplate of the apparatus was set to 33°C and the cold plate was cooled by water at 17°C. The sample was mounted between the two plates, and then, the thermal conductivity of the sample was tested when the temperatures of the two plates became stable. Here, the measurement uncertainty and repeatability of GHP were controlled within ±3% and ±1%, respectively.

3. Simulation methods

Firstly, the effective thermal conductivity (k_e) was simulated by a simulation model developed by our research group. In this simulation, k_e can be obtained as follows:

$$k_e = \frac{Q_{total} \times L}{(T_h - T_l) \times A} \tag{4}$$

where Q_{total} is the total heat flow through the sample, W; T_h and T_l were the known temperatures of the two surfaces perpendicular to the direction of heat flow, K; L is the thickness of the sample, m; and A is the area of the sample, m².

In our simulation, by comparing several grids and the results, the whole sample was finally meshed as a grid of $X \times Y \times Z$. For each axis, the grid numbers are $X = A^{0.5}$, $Y = L$, and $Z = A^{0.5}$. In addition, each unit's dimension is equalled to 0.001 m.

Then, by using the thermal conductivity matrix ($TCM = ones\ (X,\ Y,\ Z)$), each unit's thermal conductivity value was determined. For the matrix part of the sample, the thermal conductivity value of each unit is set as the thermal conductivity of the matrix board. For the foam part, the unit thermal conductivity value is set randomly. For example, there were two thermal conductivity values in the foam sample, from thermal conductivity value of the solid material and the thermal conductivity value of the air. Firstly, the volume fractions of the solid material and the air were calculated. Secondly, for each unit, a random number (rn) was generated to decide which thermal conductivity value would be endowed. For instance, for one unit,

if *rn* was smaller than the solid material's volume fraction, the thermal conductivity of the solid material would be endowed. Otherwise, this unit would be endowed with the thermal conductivity of the air (k_a = 0.026 W/(m•K) [21]).

In this simulation programme, the steady-state energy equation for three-dimensional heat transfer was established as the control equation. For each unit, the sum of heat flow towards this unit was equal to that away from it. In addition, the solution conditions were defined by using the temperature field matrix: *T = ones (X, Y, Z)*. For the surfaces perpendicular to the heat flow direction, they belonged to the first-class boundary condition and the temperatures of these two surfaces were equalled to 33°C and 17°C. As in the experiment, the sample panel was surrounded by thermal insulation fibre; similarly, the four surfaces that surrounded the panel were insulated perfectly. Finally, k_e will be obtained through the iterative calculation.

Secondly, the energy-saving effect of FCI was evaluated by EnergyPlus software [22–24]. In this research, an ideal building is applied as the calculation model for energy consumption. In addition, the energy consumption of buildings with different kinds of external walls was compared systematically.

4. Results and discussions

4.1. The properties of FCI

For the matrix part samples, the sintering temperature will have an important effect on macroscopic properties, including the moisture absorption capacity and rupture modulus, which are shown in **Figures 2** and **3**, respectively.
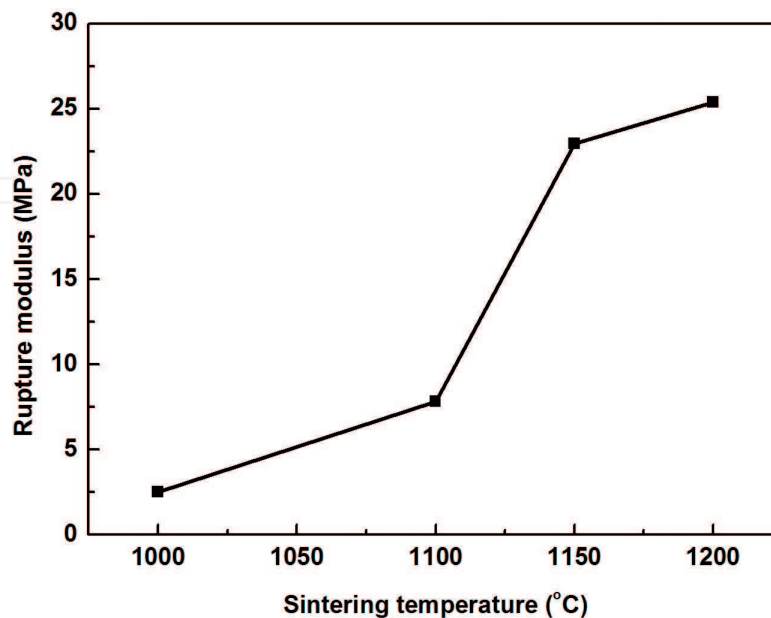

Figure 2. Rupture modulus values of the sample no. 1 versus sintering temperatures.
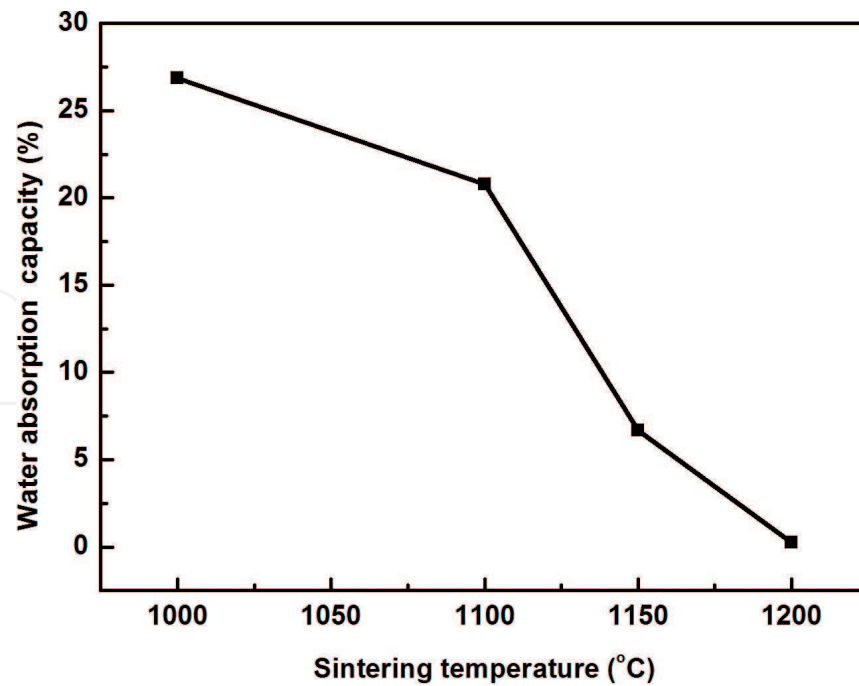
Figure 3. Moisture absorption capacity values of the sample no. 1 versus sintering temperatures.

First, the characteristic curve in **Figure 2** indicates that for the sample no.1 the rupture modulus increases with the increase of the sintering temperature. When the sintering temperature is 1000°C, the rupture modulus is only 2.52 MPa. Moreover, when the sintering temperature is increased to 1100°C, the corresponding rupture modulus increases to 7.82 MPa, indicating that there is the liquid generation in the sample no.1. Furthermore, when the sintering temperature is over 1200°C, the rupture modulus value reaches to 25.38 MPa. Second, it is interesting to note that in the investigated temperature range (1000–1200°C), the moisture absorption capacity dramatically decreases from 26.85% to 0.25% at the sintering temperature of 1000–1200°C.

It can be concluded that when the sintering temperature is 1200°C the samples have excellent properties (moisture absorption capacity and the rupture modulus), which satisfy the requirements of fine stoneware tiles [25].

In addition, the quartz was chosen as an addition to the sample no. 1. **Figures 4** and **5** show the effects of quartz addition on the sample's properties (moisture absorption capacity and rupture modulus). It can be seen that, for the sample no. 2 and no. 3, at 1200°C, the 5% and 10% quartz additions enhance the samples' strength with a little increase in moisture absorption capacity. For instance, for the sample no. 2, the highest rupture modulus reaches 34.28 MPa at 1200°C, which drastically exceeds the property of the sample no. 1 without quartz (25.38 MPa). According to the literature [26], it may be explained that, for the sample no. 2, 5% quartz addition is a benefit to the increase of mullite formation, which will promote the sample's rupture modulus. **Figure 5** shows that 5% quartz addition increases the moisture absorption capacity from 0.25 to 0.83%, but it still satisfies the standards for stoneware porcelain tiles [25].
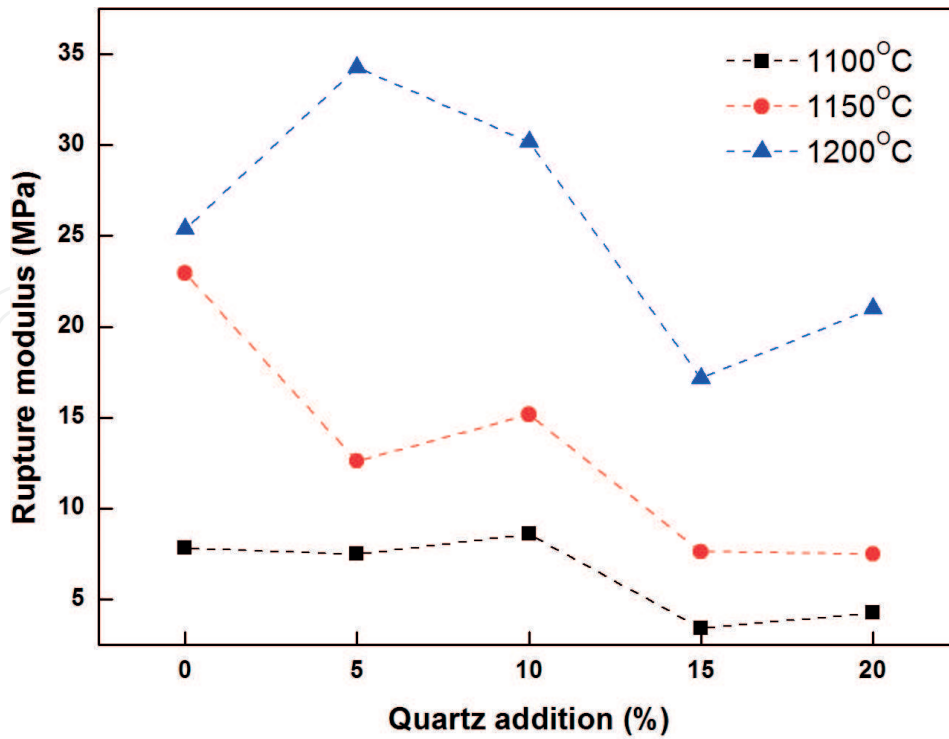
Figure 4. Rupture modulus values of the sample nos. 1–5 with different quartz addition.
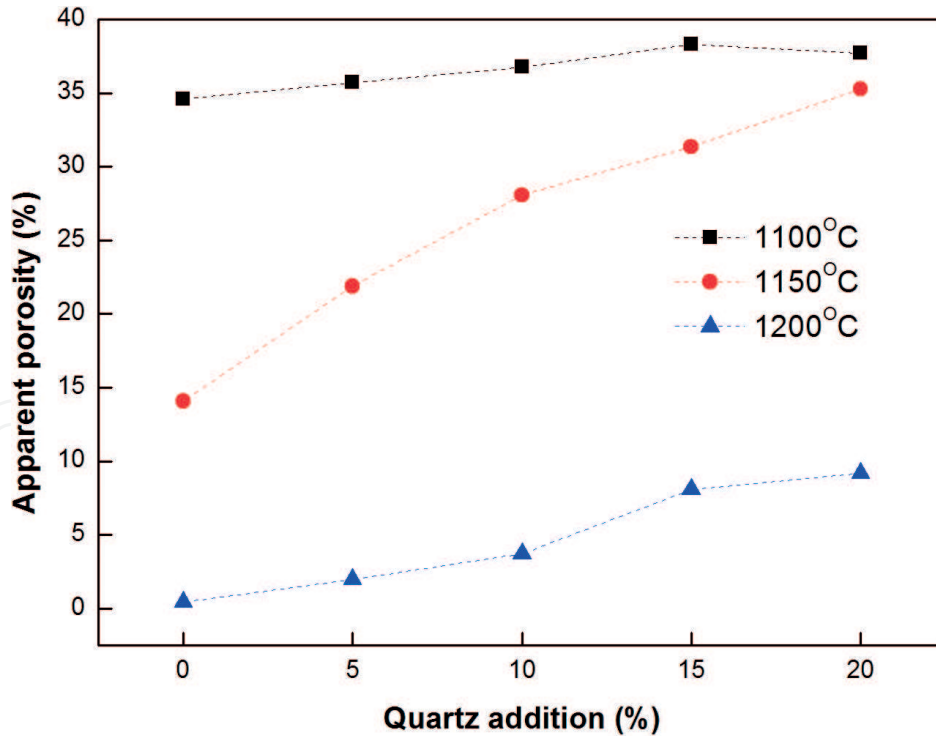

Figure 5. Moisture absorption capacity values of the sample nos. 1–5 with different quartz addition.

In order to explain the above phenomenon, the ternary diagram of sample no. 2 was calculated by FactSage. From **Figure 6**, it can be seen that the new sample's raw materials belong to SiO_2-Al_2O_3-CaO-K_2O system, as shown in red. Therefore, unlike the conventional ternary
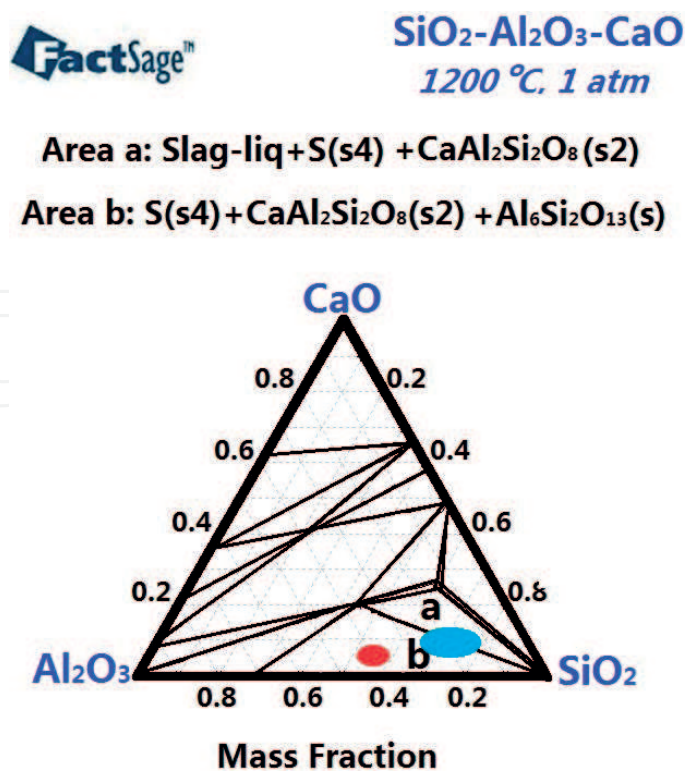
Figure 6. Ternary diagram of the traditional ceramic and sample no. 2 (blue indicates the traditional ceramic crystal phase area and red shows the phase area of sample no. 2).

ceramic system, the new sample broadens the traditional ceramic crystal phase area (blue) to a new phase area. This change of the ceramic system is due to the increase of Al_2O_3 and CaO obtained from FA.

In addition, the powder of both raw materials and sintered sample no. 2 is separately analysed by XRD. Firstly, XRD patterns in **Figure 7** depict that there is none or only a small amount of glass phase in the sintered sample no. 2, which is a benefit to the improvement of its mechanical property. The previous research [27] has shown that in the traditional porcelain stoneware tiles, glass is one of the major phases in addition to quartz and mullite. Therefore, compared to the traditional ceramic tile, the matrix part tile prepared by our research has better mechanical property. In addition, it is interesting to note that there is no quartz in sintered sample no. 2; it is replaced by a large amount of mullite, which will further promote its strength.

Moreover, **Figure 8** shows the DTA-TG curve of the sample. At 200°C, the mass loss is caused by the dehydroxylation of gypsum with an exothermic peak. At the temperature of 400–600°C, the mass loss is caused by the dehydroxylation process of boehmite (with an endothermic peak at 450°C) and kaolinite (with an endothermic peak at above 550°C). Finally, an exothermic peak at about 1000°C is attributable to mullite crystallisation [28].

Secondly, for the foam sample no. 6, the sintering temperature likewise has an important effect on the foam sample's properties, including the bulk density and volume, which are shown in **Figure 9**.
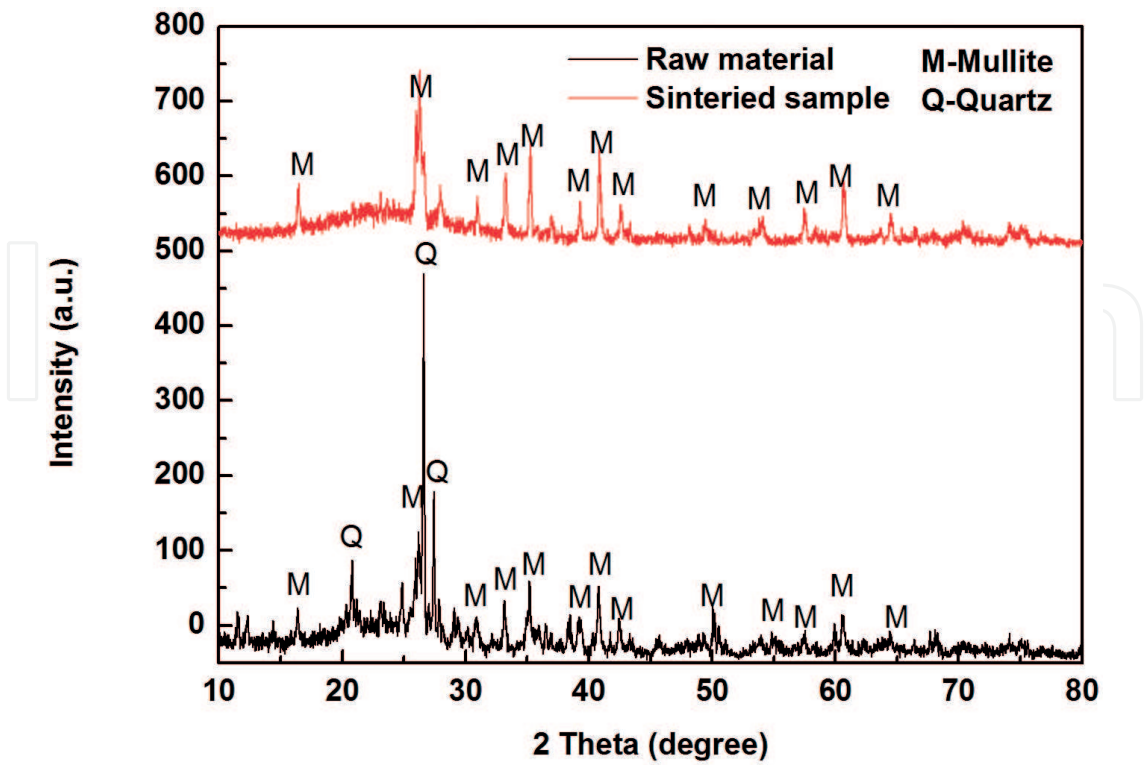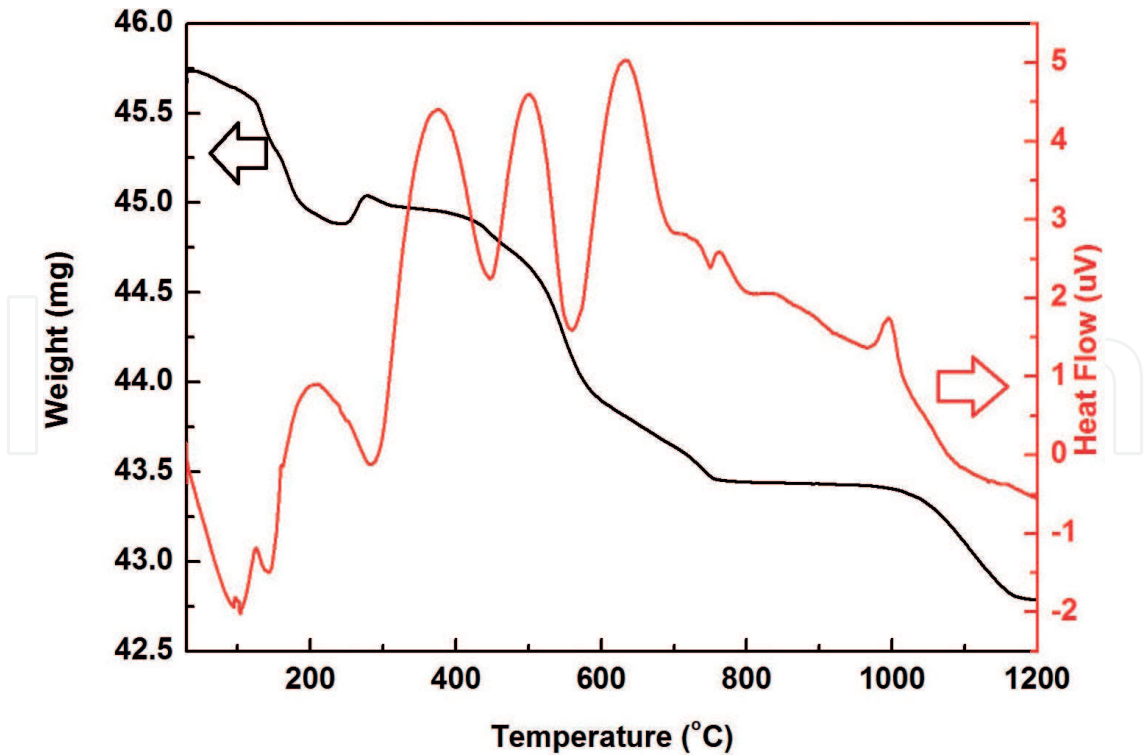
Figure 7. XRD patterns of the sample no. 2.

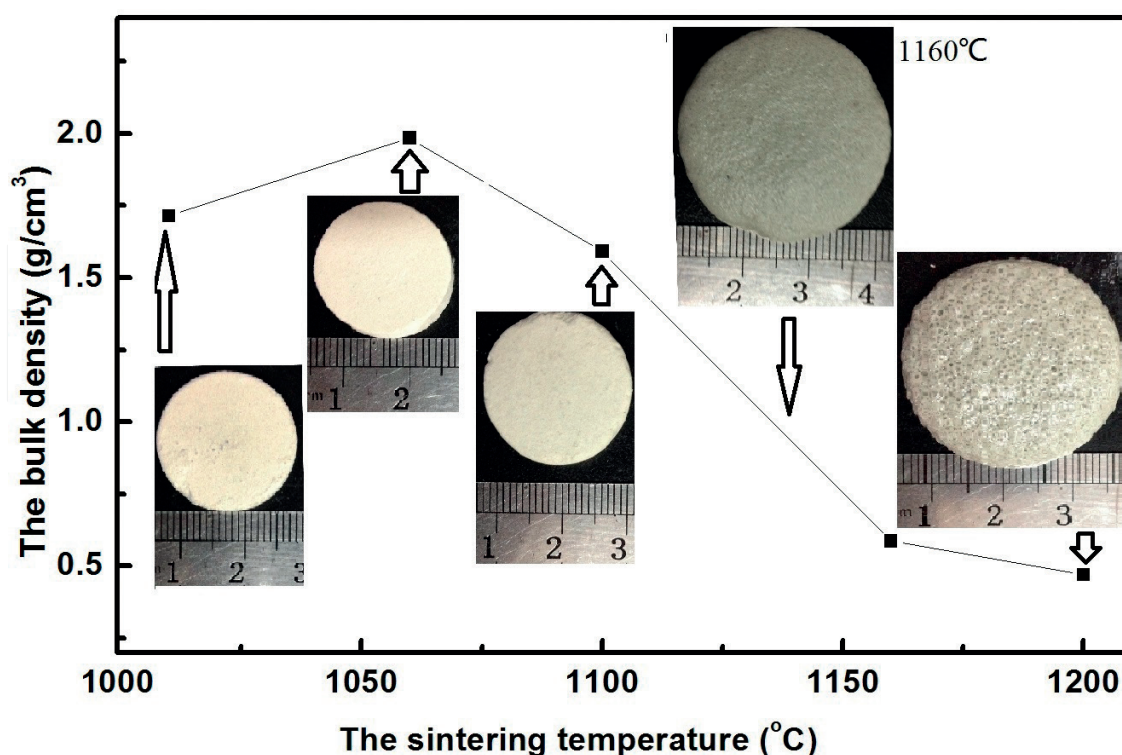**Figure 8.** DTA-TG curve of the green sample no.2.

Figure 9. The volume results and the bulk density values of the sample no. 6 at different sintering temperature.

Figure 9 indicates the effect of sintering temperature on the volume results and the bulk density values of the sample no. 6 with 1% SiC as a foaming agent. It can be seen that the volume results of the sample no. 6 first shrank and then expanded with the increase in the sintering temperature from 1010–1200°C. Therefore, it is noted that the corresponding bulk density of sample no. 6 shows a consistent trend. At 1010°C, the bulk density is 1.714 g/cm³, and then, it increases up to 1.984 g/cm³ at 1060°C, followed by a rapid decrease with further increasing sintering temperature, and reaches the minimum value of 0.471 g/cm³ at 1200°C, which is decreased by 76%.

This phenomenon is attributed to two typically changing processes in the sintering of foamed ceramics, which are matrix densification and closed-pore generation. Firstly, in the sintering process, with the increase in sintering temperature, liquid phase is generated, which led to the matrix densification [29]. Secondly, there is SiC in CW and so with the sintering temperature increase SiC began to decompose, resulting in the closed-pore generation. In the process of SiC decomposition, the gas (CO_2 or CO) is generated in the presence of oxygen, which is shown in **Figure 10** [30–32].

Moreover, the measured thermal conductivity of the sample no. 6 as a function of the bulk density is demonstrated in **Figure 11**. It can be seen that the measured thermal conductivity decreases from 0.3876 W/(m•K) to 0.1184 W/(m•K) with the increase in the bulk density of the sample no. 6. It is concluded that the sample no. 6 at high sintering temperature (1200°C) has an excellent heat insulation performance, indicating that it can be utilised as the foam part of FCI.
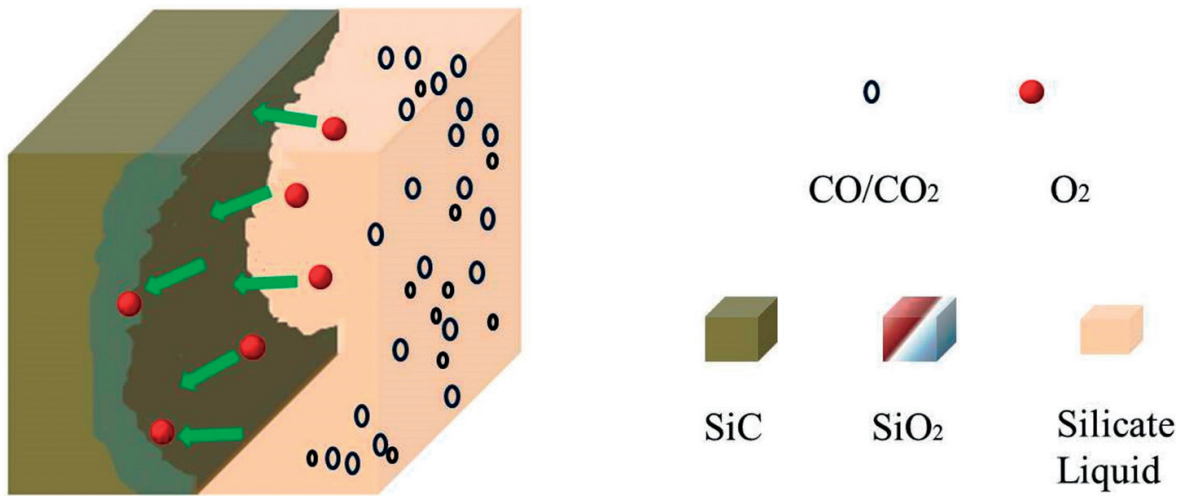
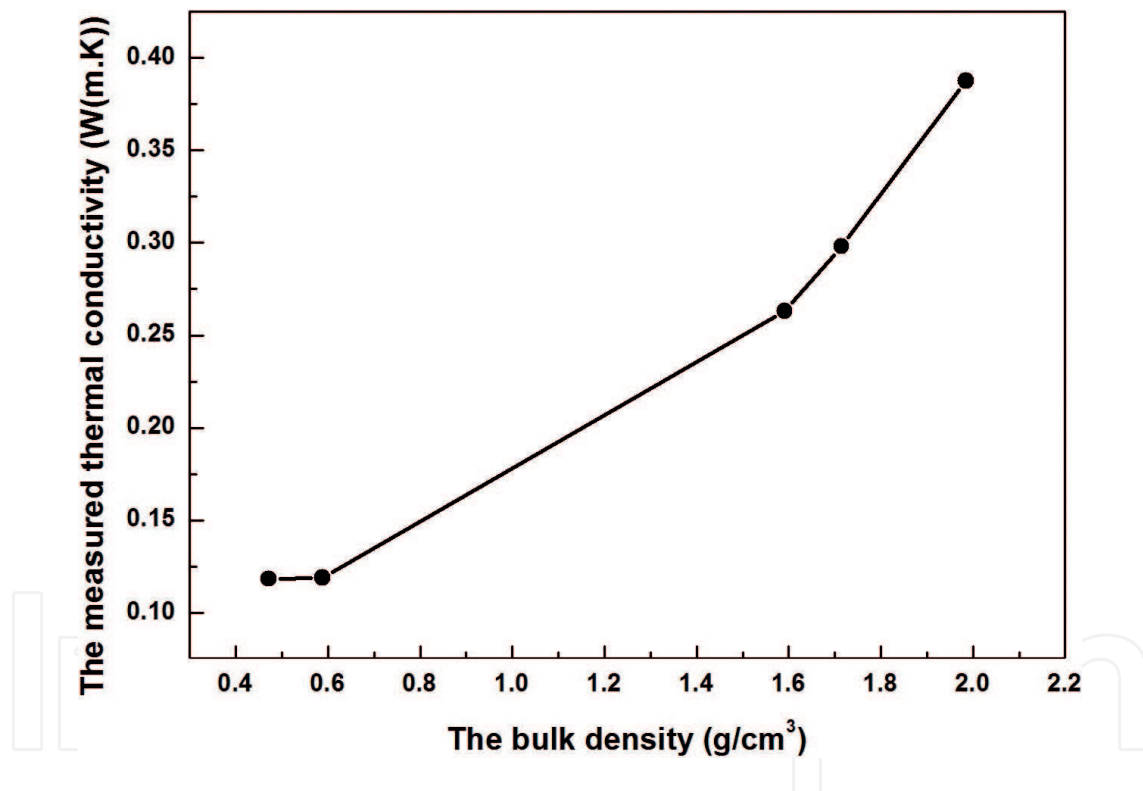**Figure 10.** The reaction principle of SiC as a foaming agent.

Figure 11. The measured thermal conductivity of the sample no. 6 as a function of the bulk density.

4.2. The forecast of the thermal conductivity and energy saving of FCI

4.2.1. Numerical simulation results of the effective thermal conductivity

The relationship between the effective thermal conductivity and the bulk density can be calculated through the present proposed model. The results of the effective thermal conductivity, k_e, as a function of the bulk density, are indicated in **Figure 12**. It can be seen that the effective thermal conductivity decreases with the decrease of the bulk density. It is interesting
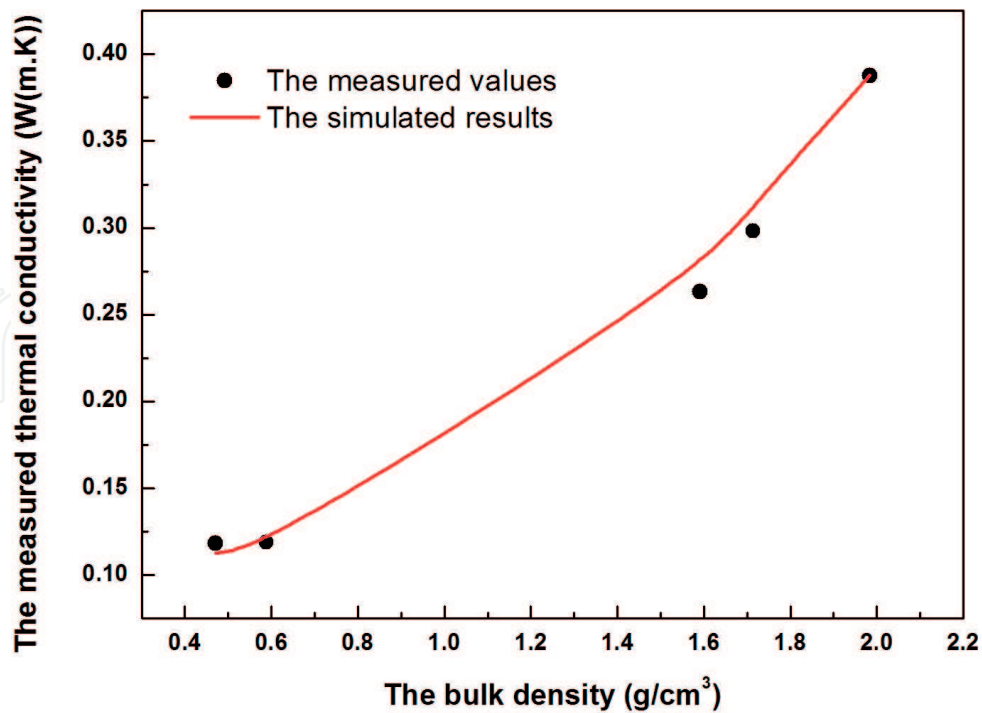
Figure 12. The simulation results of the effective thermal conductivity of the sample no. 6 as a function of the bulk density.

to note that, when the bulk density continues decreasing to a certain level (1.600 g/cm^3), the decrease rate of the effective thermal conductivity becomes small. In addition, it can be seen that the simulated effective thermal conductivities are well in agreement with the measured effective thermal conductivities, with the average deviation of 4%.

From **Figure 12**, we can also get the following relationship between the effective thermal conductivity and the bulk density for the foam sample at 25°C.

$$k_e = 0.15002 - 1.25 \times 10^{-4} \rho_b + 1.23 \times 10^{-7} \rho_b^2 \tag{5}$$

4.2.2. The forecast of the energy saving of FCI in an ideal building

In this part, a building (3 m*3 m*2.8 m) in Beijing is used as the calculation model for energy consumption (**Figure 13(a)**). In this building model, there are two kinds of external walls, traditional wall and foam ceramic insulation wall. As shown in **Figure 13(b)**, the foam ceramic insulation wall is composed of four layers: the cement mortar (20 mm, 0.97 W/(m•K)), the matrix part of the foam ceramic insulation (200 mm), the foam part of the foam ceramic insulation (50 mm), and the composite mortar (20 mm, 0.65 W/(m•K)). For the traditional wall, the matrix and foam parts of the foam ceramic insulation were removed and were replaced with a 250-mm reinforced concrete with the thermal conductivity of 1.95 W/(m•K).

Figure 14 shows the annual energy consumption for the ideal building with different external walls. It can be seen that, compared with the traditional wall, the FCI wall significantly reduces the annual energy consumption by 44–57%. In addition, for the building with FCI wall, the annual average heating and cooling rate decreases with the decrease in the bulk
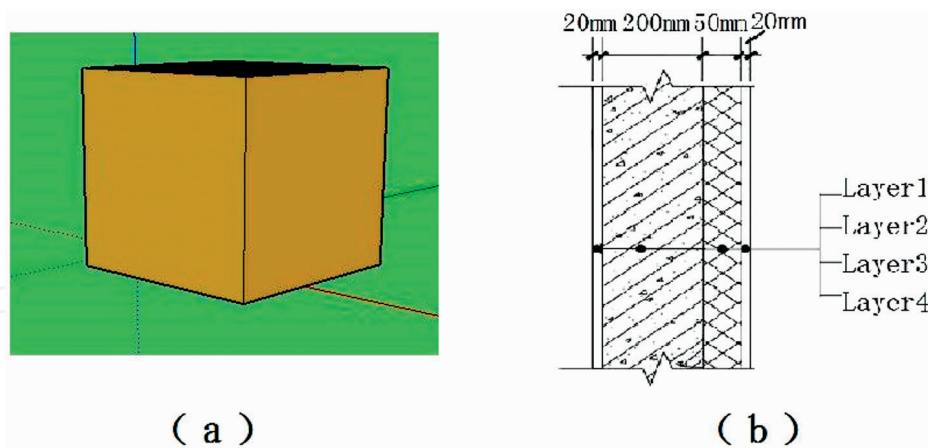
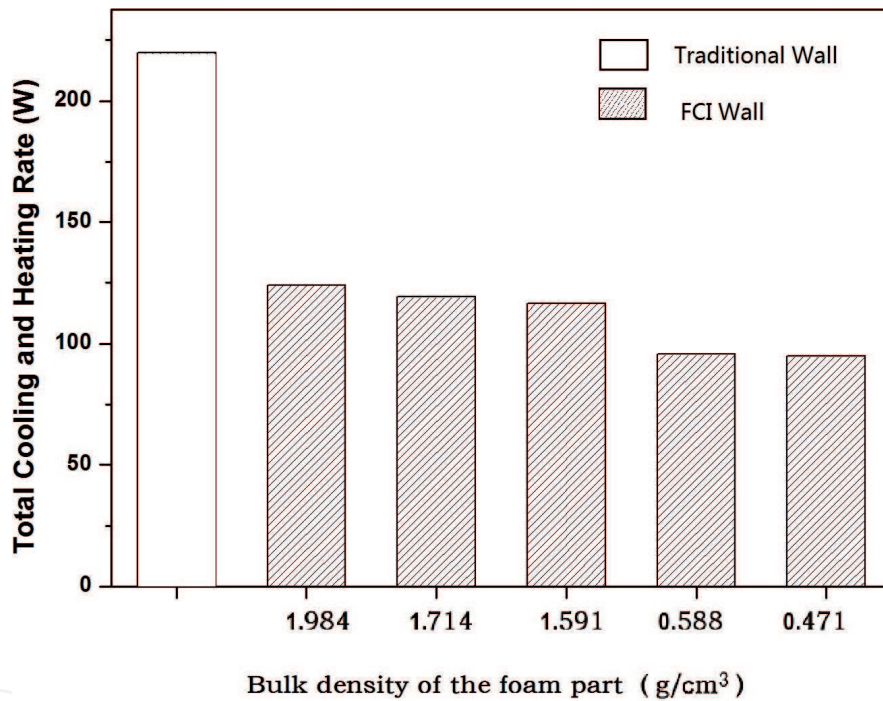**Figure 13.** The ideal calculation building model.

Figure 14. Heating and cooling annual loads in ideal building with different external walls.

density of the foam part of FCI. For instance, when ρ_b = 0.471 g/cm³, for the ideal building the annual average heating and cooling rate is only 95 W, and compared with that of the building with a traditional wall, the rate is reduced by 57%. Therefore, the energy conservation of the FCI wall is especially pronounced.

5. Conclusion

In this research, solid wastes, such as FA and CW, were effectively utilised for the manu-facture of FCI, leading to low-cost and environmental protection. The experiment and

simulation methods are applied to study the effects of sintering temperature and the additive agent on properties of the samples.

For the matrix part of FCI, at 1200°C, the sample with 50 wt% FA and 5 wt% quartz addition shows the best complex properties. The rupture modulus is 34.28 MPa, and the corresponding moisture absorption capacity is only 0.83%. In addition, for the foam sample with 1 wt% silicon carbide, the lowest bulk density and thermal conductivity at 1200°C are 0.471 g/cm^3 and 0.1184 W/(m•K), respectively.

Moreover, the thermal conductivities of CFI and its effect on energy saving in buildings were simulated by a simulation model and EnergyPlus, respectively. Firstly, the proposed simulation model was applied to predict the effective thermal conductivity of the sample no. 6 as a function of bulk density. The simulation results show that the effective thermal conductivity of the sample no. 6 decreases with the decrease in its bulk density, and the simulation values are in good agreement with the measured results, with an average deviation of 4%. These simulation methods are desirable not only for the practical purpose of predicting the thermal properties of CFI, but also for the fundamental knowledge required in developing other new porous ceramics. Furthermore, the EnergyPlus results indicate that FCI can efficiently reduce the thermal load caused by the heat loss of the external construction, so the proposed FCI exhibits excellent energy conservation effect.

Acknowledgements

Author details

Ru Ji[1]*, Xidong Wang[2] and Yang He[3]

*Address all correspondence to: jiru@ustb.edu.cn

1 School of Civil and Resource Engineering, University of Science and Technology Beijing, Beijing, The People's Republic of China

2 Department of Energy and Resources Engineering and Beijing Key Laboratory for Solid Waste Utilization and Management, College of Engineering, Peking University, Beijing, The People's Republic of China

3 Nuclear Power (Bidding) Dept. 1, China Nuclear Energy Industry Corp., Beijing, The People's Republic of China

References

[1]   Domínguez A, Domínguez MI, Ivanova S, et al. Recycling of construction and demolition waste generated by building infrastructure for the production of glassy materials. Ceramics International. 2016;**42**(14):15217-15223

[2]   Hsu D. Comparison of integrated clustering methods for accurate and stable prediction of building energy consumption data. Applied Energy. 2015;**160**:153-163

[3]   Huebner GM, Hamilton I, Chalabi Z, et al. Explaining domestic energy consumption: The comparative contribution of building factors, socio-demographics, behaviours and attitudes. Applied Energy. 2015;**159**:589-600

[4]   Taurino R, Barbieri L, Bondioli F. Surface properties of new green building material after TiO2–SiO2, coatings deposition. Ceramics International. 2015;**42**(4):4866-4874

[5]   Dan D, Tanasa C, Stoian V, et al. Passive house design-an efficient solution for residential buildings in Romania. Energy for Sustainable Development. 2016;**32**:99-109

[6]   Al-Homoud MS. Performance characteristics and practical applications of common building thermal insulation materials. Building and Environment. 2005;**40**(3):353-366

[7]   Bobkova NM, Barantseva SE, Trusova EE. Production of foam glass with granite siftings from the Mikashevichi deposit. Glass and Ceramics. 2007;**64**(1-2):47-50

[8]   Fraga D, Lyubenova TS, Martí R, et al. Ecologic ceramic substrates for CIGS solar cells. Ceramics International. 2016;**42**(6):7148-7154

[9]   Andreola F, Barbieri L, Lancellotti I, et al. Recycling of industrial wastes in ceramic manufacturing: State of art and glass case studies. Ceramics International. 2016;**42**(12): 13333-13338

[10] Pérez JM, Romero M. Microstructure and technological properties of porcelain stoneware tiles moulded at different pressures and thicknesses[J]. Ceramics International. 2014;**40**(1):1365-1377

[11] Zhu M, Ji R, Li Z, et al. Preparation of glass ceramic foams for thermal insulation applications from coal fly ash and waste glass. Construction and Building Materials. 2016;**112**: 398-405

[12] Ji R, Zhang Z, He Y, et al. Synthesis, characterization and modelling of new building insulation material using ceramic polishing waste residue. Construction and Building Materials. 2015;**85**:119-126

[13] Ji R, Zhang Z, Yan C, et al. Preparation of novel ceramic tiles with high Al 2 O 3, content derived from coal fly ash. Construction and Building Materials. 2016;**114**:888-895

[14] Lizarazo-Marriaga J, García F, Higuera C. Preliminary electrochemical cementation of high volume fly ash mortars. Construction and Building Materials. 2016;**122**:54-62

[15] Zhu M, Ji R, Li Z, et al. Preparation of glass ceramic foams for thermal insulation applications from coal fly ash and waste glass. Construction and Building Materials. 2016;**112**: 398-405

[16] Luo Y, Ma S, Zhao Z, et al. Preparation and characterization of whisker-reinforced ceramics from coal fly ash. Ceramics International. 2016;**43**(1):1-11

[17] Zhu L, Dong Y, Li L, et al. Coal fly ash industrial waste recycling for fabrication of mullite-whisker-structured porous ceramic membrane supports. RSC Advances. 2015;**5**(15): 11163-11174

[18] Silvestre R, Medel E, García A, Navas J. Using ceramic wastes from tile industry as a partial substitute of natural aggregates in hot mix asphalt binder courses. Construction and Building Materials. 2013;**45**:115-122

[19] Higashiyama H, Yamauchi K, Sappakittipakorn M, Sano M, Takahashi OA. Visual investigation on chloride ingress into ceramic waste aggregate mortars having different water to cement ratios. Construction and Building Materials. 2013;**40**:1021-1028

[20] Pereira-de-Oliveira LA, Castro-Gomes JP, Santos P. The potential pozzolanic activity of glass and red-clay ceramic waste as cement mortars components. Construction and Building Materials. 2012;**31**:197-203

[21] Bomberg M, Klarsfeld S. Semi-empirical model of heat transfer in dry mineral fiber insulations. Journal of Building Physics. 1983;**6**(3):156-173

[22] Crawley DB, Lawrie LK, Winkelmann FC, Buhl WF, Huang YJ, Pedersen CO. EnergyPlus: Creating a new-generation building energy simulation program. Energy and Buildings. 2001;**33**(4):319-331

[23] Fumo N, Mago P, Luck R. Methodology to estimate building energy consumption using EnergyPlus benchmark models. Energy and Buildings. 2010;**42**(12):2331-2337

[24] Miyazaki T, Akisawa A, Kashiwagi T. Energy savings of office buildings by the use of semi-transparent solar cells for windows. Renewable Energy. 2005;**30**(3):281-304

[25] State general administration of the People's Republic of China for quality supervision and inspection and quarantine. Ceramic tiles, GB/T4100-2006. Beijing: Standards Press of China; 2006 [Chinese]

[26] Mah T-I, Mazdiyasni KS. Mechanical properties of Mullite. Journal of the American Ceramic Society. 1983;**66**(10):699-703

[27] Martín-Márquez J, Rincón JM, Romero M. Effect of firing temperature on sintering of porcelain stoneware tiles. Ceramics International. 2008;**34**(8):1867-1873

[28] Lee WE, Souza GP. Mullite formation in clays and clay-derived vitreous ceramics. Journal of the European Ceramic Society. 2008;**28**(2):465-471

[29] Amorós JL, Orts MJ, García-Ten J, Gozalbo A, Sánchez E. Effect of the green porous texture on porcelain tile properties. Journal of the European Ceramic Society. 2007;**27**(5): 2295-2301

[30] García-Ten J, Saburit A, Bernardo E, Colombo P. Development of lightweight porcelain stoneware tiles using foaming agents. Journal of the European Ceramic Society. 2012;**32**(4):745-752

[31] Bernardin AM, Silva MJ, Riella HG. Characterization of cellular ceramics made by porcelain tile residues. Materials Science and Engineering A. 2006;**437**(2):222-225

[32] Orts MJ, Amorós JL, Escardino A, Gozalbo A, Feliu C. Kinetic model for the isothermal sintering of low porosity floor tiles. Applied Clay Science. 1993;**8**(2):231-245